molecular pharmaceutics

Article

pubs.acs.org/molecularpharmaceutics

# Tobacco Mosaic Virus-Delivered Cisplatin Restores Efficacy in Platinum-Resistant Ovarian Cancer Cells

Christina E. Franke,[†] Anna E. Czapar,[‡] Ravi B. Patel,[§] and Nicole F. Steinmetz*[,†,∥,⊥,#,▽]

[†]Departments of Biomedical Engineering, [‡]Pathology, [§]Radiation Oncology, [∥]Radiology, [⊥]Materials Science and Engineering, [#]Macromolecular Science and Engineering, and [▽]Division of General Medical Sciences-Oncology, Case Comprehensive Cancer Center, Case Western Reserve University Schools of Medicine and Engineering, Cleveland, Ohio 44106, United States

**ABSTRACT:** Platinum resistance in ovarian cancer is the major determinant of disease prognosis. Resistance can first appear at the onset of disease or develop in response to platinum-based chemotherapy. Due to poor response to alternate chemotherapies and lack of targeted therapies, there is an urgent clinical need for a new avenue toward treatment of platinum-resistant (PR) ovarian cancer. Nanoscale delivery systems hold potential to overcome resistance mechanisms. In this work, we present tobacco mosaic virus (TMV) as a nanocarrier for cisplatin for treatment of PR ovarian cancer cells. The TMV-cisplatin conjugate (TMV-cisPt) was synthesized using a charge-driven reaction that, like a classic click reaction, is simple and reliable for large-scale production. Up to ∼1900 cisPt were loaded per TMV-cisPt with biphasic release profiles characterized by a fast half-life ($t_1$) of ∼1 h and slow half-life ($t_2$) of ∼12 h independent of pH. Efficient cell uptake of TMV was observed when incubated with ovarian cancer cells, and TMV-cisPt demonstrated superior cytotoxicity and DNA double strand breakage (DSB) in platinum-sensitive (PS) and PR cancer cells when compared to free cisplatin. The cytotoxicity in PR ovarian cancer cells and overall lower effective dosage requirement makes TMV-cisPt a powerful candidate for improved ovarian cancer treatment strategies.

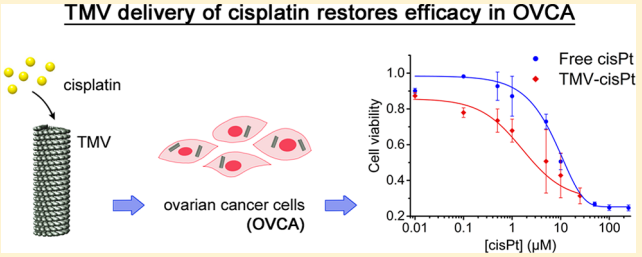


**KEYWORDS:** *nanotechnology, nanoparticles, plant viruses, drug delivery, drug resistance, tobacco mosaic virus, cisplatin, platinum therapy, platinum resistance, chemotherapy, ovarian cancer*

## INTRODUCTION

Ovarian cancer is the most fatal gynecologic malignancy, and epithelial ovarian cancer is the fourth leading cause of cancer-related death in women.[1] This high rate of mortality is largely due to the high occurrence of late-stage diagnosis, when metastases are already present in the abdomen. Compared to localized disease, which has a five-year relative survival rate of 92%, disseminated, metastatic disease has a five-year survival rate of only 28%.[2] Although more than 75% of patients achieve complete remission after cytoreductive surgery and platinum-based chemotherapy, this initial sensitivity declines with repeated treatments, and platinum-resistant (PR) cancer stem cells may remain in the intraperitoneal (IP) space, undetected.[3] As a result, 75% of patients diagnosed with advanced ovarian cancer will develop recurrent disease within five years, upon which their prognosis declines significantly.[1−4]

Since recurrent ovarian cancer is usually incurable, additional treatments administered to patients with recurrent disease are palliative rather than curative; patients with platinum-sensitive (PS) recurrent disease have a median survival of only 3 years, and the median survival from diagnosis of PR disease is 1 year.[1,5] The available treatment options are suboptimal; PS ovarian cancer is repeatedly treated with platinum therapy until development of PR disease, and, as there is no established treatment for PR ovarian cancer, it is typically treated using experimental drugs and therapies under development in clinical trials. Therapeutic options that have been previously tested include PEGylated liposomal doxorubicin, topotecan, and emicitabine; nevertheless these approaches achieved low response rates.[1,2] This poor prognosis and current lack of alternate effective treatment approaches to front-line platinum therapies demonstrates that there is clinical demand for novel drug formulations with improved efficacy against PS and PR cancer cells during initial treatment as well as for resensitization of PR cells.

For all stages of ovarian cancer, platinum sensitivity remains the major determinant of patient prognosis, as the standard-of-care is platinum-based combination therapy. Cisplatin (*cis*-$[Pt(NH_3)_2Cl_2]$, cisPt) is the most common drug used for intraperitoneally administered ovarian cancer therapy; it is also used in the setting of testicular and bladder cancer.[6,7] Typically, cisplatin, or its less toxic analogue, carboplatin, are administered in combination with a taxane chemotherapeutic such as paclitaxel.[8] While cisplatin and carboplatin demonstrate

**Special Issue:** Click Chemistry for Medicine and Biology

**Received:** June 7, 2017
**Revised:** September 6, 2017
**Accepted:** September 7, 2017





DOI: 10.1021/acs.molpharmaceut.7b00466
*Mol. Pharmaceutics* XXXX, XXX, XXX−XXX

equivalent efficacy in intravenous treatment,[9] cisplatin is associated with greater toxicity. However, cisplatin offers greater efficacy than carboplatin in intraperitoneal (IP) administration, which is preferred for the treatment of late-stage ovarian cancers exhibiting IP metastases.[10,11] Cisplatin, therefore, is the drug of choice for this study.

Despite powerful inducement of intrastrand DNA cross-links leading to potent genotoxicity, administration of unprotected "free" platinum drugs leads to nonspecific, dose-limiting toxicity, notably nephrotoxicity, neurotoxicity, and myelosuppression.[12] Thus, a drug delivery formulation that would specifically deliver a cisplatin payload to cancer cells, even in cases of platinum-resistance, would not only reduce the toxic side effects of cisplatin therapy in ovarian cancer patients but would also make strides toward a curative rather than palliative treatment for a broad range of refractory malignancies. For this reason, a variety of nanoparticle platforms have been explored for delivery of cisplatin; to date, however, few efforts have focused on treatment of PR ovarian cancer cells; instead, many formulations are tested in lung, head and neck, colorectal, and prostate cancers.[12−14] Of the nanoparticle platforms developed for ovarian cancer treatment, many are centered on delivery of nucleic acid therapies such as siRNA and gene inhibitors.[15]

In this work, we present a plant virus-based nanoparticle system for delivery of cisplatin; we evaluate efficacy of the approach using PS and PR ovarian cancer cells. The utility of virus nanoparticles for biomedical applications has been reviewed elsewhere;[16] some approaches make use of viruses' natural ability to insert therapeutic genetic materials into target cells[17,18] while other applications build on the use of noninfectious plant viruses or bacteriophages as carriers for therapeutics.[19−21] While gene therapies have already advanced to clinical settings, applications with plant viruses and bacteriophages remain in the preclinical development phase. Here, we chose a plant virus-based platform based on their high degree of biocompatibility and biodegradability as well as their monodispersity and potential for scalable manufacturing in plants.[19,22,23]

Many virus-based delivery systems take advantage of available amino acid residues on some viral capsid proteins which enable selective modification of interior and exterior surfaces for tunable properties.[20,21] Using this strategy we have previously demonstrated that a variety of pharmaceuticals[24−28] and imaging contrast agents[29] can be effectively delivered by plant virus-based nanoparticles to breast, melanoma, ovarian, and prostate cancers, among other malignancies. Our cisplatin delivery system described in this work makes use of the nucleoprotein components of the tobacco mosaic virus (TMV), a high-aspect-ratio, hollow cylindrical nanoparticle platform with dimensions of 300 × 18 nm and an interior channel 4 nm in diameter.[26] Cisplatin-loaded TMV, termed TMV-cisPt, was synthesized, and stability of the formulation and cisplatin-release profiles were analyzed. Finally, efficacy of TMV-cisPt in PS and PR epithelial ovarian cancer cells was evaluated; we determined the $IC_{50}$ of the TMV-cisPt formulation and also gained insights into the mechanism of action.

## EXPERIMENTAL SECTION

**Materials.** All reagents and buffers were purchased from Fisher Scientific (Fairlawn, NJ) unless otherwise specified. Cisplatin was purchased from Tocris Bioscience (Bristol, UK). ACS grade silver nitrate (99.9+% purity) was purchased from Alfa Aesar (Ward Hill, MA). *N*-(3-(Dimethylamino)propyl)-*N*′-ethylcarbodiimide hydrochloride (EDC) and propargylamine were purchased from Sigma-Aldrich (St. Louis, MO). Sulfo-cyanine5 azide was purchased from Lumiprobe (Hallandale Beach, FL). Paraformaldehyde (10% v/v) and glutaraldehyde (25% v/v) were purchased from Electron Microscopy Sciences (Hatfield, PA). Triton X-100 was purchased from United States Biochemical Corporation (Salem, MA). Custom rabbit anti-TMV primary antibody was purchased from Pacific Immunology (Ramona, CA). Alexa Fluor 488 antihuman CD107a (LAMP-1) antibody was purchased from BioLegend (San Diego, CA). Fluoroshield mounting medium with DAPI (4′,6-diamidino-2-phenylindole) was purchased from Sigma-Aldrich (St. Louis, MO). MTT cell proliferation assay kit was purchased from Trevigen (Gaithersburg, MD). Mouse monoclonal antiphospho-histone H2AX antibody was purchased from Millipore (Darmstadt, Germany). Dulbecco's Modified Eagle Medium (DMEM, 1X), penicillin/streptomycin, and 0.05% trypsin-EDTA (1X) were purchased from Life Technologies Corporation (Grand Island, NY). RPMI 1640 (1X) and phosphate-buffered saline (PBS) without calcium and magnesium were purchased from Mediatech, Inc., (Manassas, VA). Bovine serum albumin was purchased from Research Products International Corporation (Mt. Prospect, IL).

**Synthesis of TMV-cisPt.** TMV was produced in *Nicotiana benthamiana* plants using established protocols.[30] Positively charged cisPt+ was obtained by allowing cisPt to react overnight at a concentration of 1 mg/mL with $AgNO_3$ (1.97 equiv),[31] forming a white AgCl precipitate. The precipitate was then removed by two cycles of centrifugation at 14 000 *g* for 10 min. Immediately following purification, TMV-cisPt was produced using a reliable one-step aqueous reaction that meets the simplicity requirements for click chemistry defined by Sharpless and Finn.[32] Loading of cisPt+ into TMV was achieved by mixing cisPt+ and TMV for 2 h at room temperature in borate buffer (0.01 M). TMV was kept at a concentration of 1 mg/mL; pH (7.4, 7.8, and 8.2) and molar equivalents of cisplatin (5k, 10k, and 20k) were tested as variable parameters to optimize loading. These loading conditions were tested in triplicate with cisPt+ and unmodified cisPt in parallel. Unbound excess cisplatin was removed by ultracentrifugation for 1 h at 160 000 *g* (Beckman Coulter) over a 40% (w/v) sucrose cushion; TMV-cisPt was recovered in potassium phosphate (KP) buffer (0.01 M, pH 7.4). Platinum concentration was determined using graphite furnace atomic absorption spectrometry at the wavelength 265 nm (GF-AAS, FS220, Varian), and TMV concentration was determined by UV−vis (NanoDrop 2000, Thermo Scientific). Structural integrity of TMV-cisPt was verified using transmission electron microscopy (TEM, Tecnai) and staining with 2% uranyl acetate.

**Cisplatin Release Profile.** To determine the profile of cisplatin release from TMV, TMV-cisPt was dialyzed at room temperature against PBS (0.01 M) pH-adjusted with HCl to pH 7.4 and 5.4 using Slide-A-Lyzer MINI dialysis tubes (MWCO 10 kDa, ThermoFisher). Fractions of TMV-cisPt were collected immediately after immersion and every few hours over the course of 72 h, and remaining cisplatin content was measured using GF-AAS and UV−vis as described above.

**Cell Culture.** A2780 (untreated ovarian cancer) and OVCAR3 (refractory ovarian cancer) cell lines were a generous gift from Dr. DiFeo, Case Western Reserve University. A2780 and OVCAR3 were cultured in DMEM and RPMI, respectively, supplemented with 10% (v/v) fetal bovine


DOI: 10.1021/acs.molpharmaceut.7b00466
Mol. Pharmaceutics XXXX, XXX, XXX−XXX

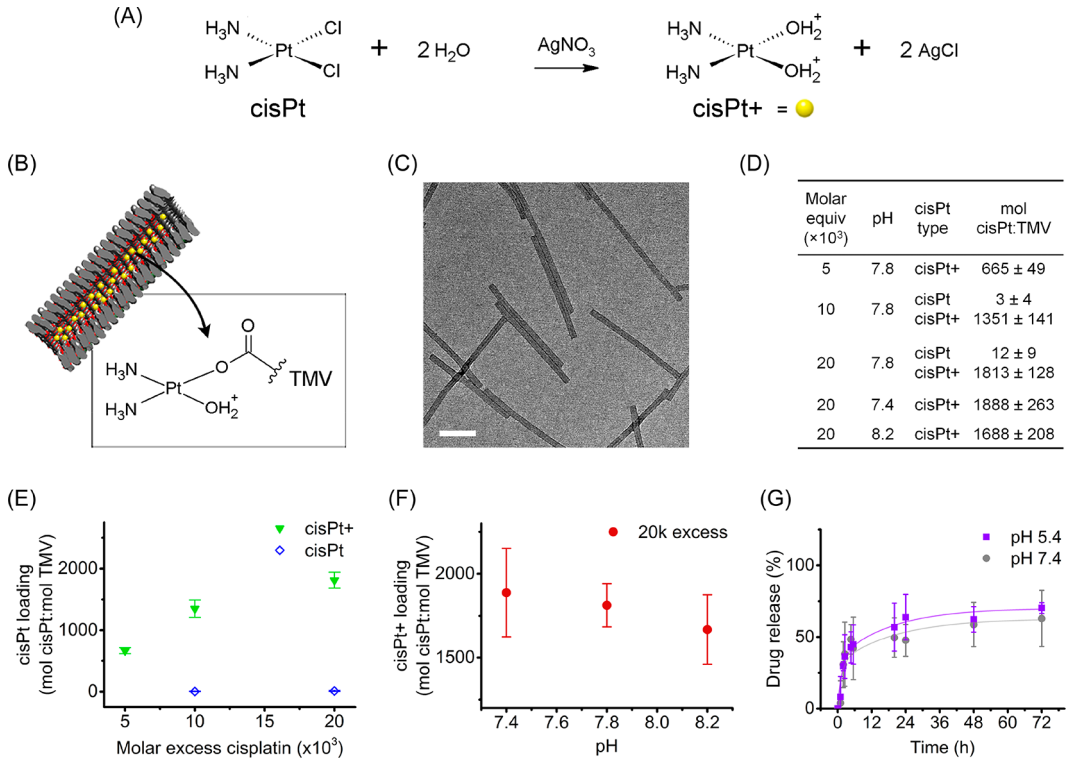


**Figure 1.** Synthesis and characterization of TMV-cisPt. (A) Structures of cisPt and cisPt+ and reaction scheme to produce cisPt+. (B) Schematic of cisPt encapsulation in interior TMV channel with expected dominant chemical structure shown. Longitudinal cross-section of TMV-cisPt is shown with interior glutamic acid residues highlighted in red. Molecular graphics images were produced using the UCSF Chimera package from the Computer Graphics Laboratory, University of California, San Francisco (supported by NIH P41 RR-01081).[39] (C) TEM image demonstrating structural integrity of TMV-cisPt (scale bar 100 nm). (D) Cisplatin load per TMV as a function of cargo (cisPt vs cisPt+), pH, and molar excess of cisPt(+):TMV (experiments were performed in triplicates and repeated at least once; the mean ± SD is plotted). (E) TMV-cisPt loading results comparing cisPt and cisPt+ at various molar excess. (F) Loading of cisPt+ at various pH. (G) Cumulative release profile of TMV-cisPt+ at pH 5.4 and 7.4 in PBS (experiments were performed in triplicates and repeated twice; the mean ± SD is plotted).

serum (FBS) and 1% (v/v) penicillin/streptomycin. Cells were maintained at 37 °C and 5% $CO_2$.

**TMV−Cell Interactions by Flow Cytometry and Fluorescence Microscopy.** Fluorescently labeled TMV (TMV-Cy5) was synthesized as previously described.[33] In brief, an alkyne group was introduced to the TMV interior channel using EDC coupling between interior glutamic acids and propargylamine (at a molar excess of 25 to 1 TMV coat protein) overnight in HEPES buffer (0.01 M, pH 7.4). The resulting TMV was reacted by Cu(II)-catalyzed azide−alkyne cycloaddition (CuAAC) click reaction with Sulfo-Cy5 azide (at a molar excess of 5 to 1 TMV coat protein) in KP buffer (0.01 M, pH 7.4) for 30 min at 4 °C. The reaction was stopped with EDTA, and TMV-Cy5 particles were purified by ultracentrifugation for 1 h over 40% (w/v) sucrose. Conjugation of Cy5 to TMV was verified using UV−vis and SDS-PAGE. Hydrodynamic radii of TMV-Cy5 and unmodified TMV were estimated using dynamic light scattering (DLS).

A2780 and OVCAR3 cells were used for flow cytometry analysis and uptake experiments; all experiments were performed in triplicate and repeated at least once. Cells were prepared for flow cytometry using established methods;[34] cells were washed in PBS and collected using enzyme-free Hank's based cell dissociation buffer. 1 ×$10^6$ cells/well were added to V-bottom 96-well plates and immediately incubated with 1 × $10^5$ particles/cell. After 15 h, excess TMV was removed by washing twice in FACS buffer. Cells were fixed for 15 min in 2% (v/v) paraformaldehyde and washed twice more before being resuspended in 100 μL FACS buffer and stored at 4 °C until analysis. 10 000 events were recorded for each sample using the Attune NxT flow cytometer (Life Technologies) and analyzed using FlowJo 10.2 software to determine the percentage of cells that stained positive for fluorescent TMV-Cy5.

For fluorescence microscopy, A2780 cells were plated at 2.5 × $10^4$ cells/well in triplicate on 1.5 mm thick coverslips placed in a 24-well plate 24 h prior to the experiment. Cells were incubated for 24 h with 2.5 × $10^6$ TMV/cell. According to protocol previously established,[33] cells were fixed in 4% (v/v) paraformaldehyde and 0.3% (v/v) glutaraldehyde in PBS and washed three times in PBS between all steps. All staining agents were diluted in 5% (v/v) goat serum albumin (GSA) in PBS. Cell membranes were stained with Alexa Fluor 555-conjugated wheat germ agglutinin (1:1000 dilution). Cells were then permeabilized in 0.2% (v/v) Triton X-100 in PBS, blocked in 10% (v/v) GSA, and stained for TMV and endolysosomes. TMV was stained using rabbit anti-TMV primary antibody (1:200 dilution) and Alexa Fluor 488 goat antirabbit IgG secondary (1:1000 dilution); endolysosomes were stained using mouse antihuman CD107a (LAMP-1) primary antibody (1:200 dilution) and Alexa Fluor 647 goat antimouse IgG secondary (1:500 dilution). Coverslips were mounted onto slides using mounting medium with DAPI to stain nuclei. Fluorescent images were obtained using Zeiss Axio Imager Z1 fluorescent inverted high-resolution microscope with motorized stage. The


DOI: 10.1021/acs.molpharmaceut.7b00466
Mol. Pharmaceutics XXXX, XXX, XXX−XXX

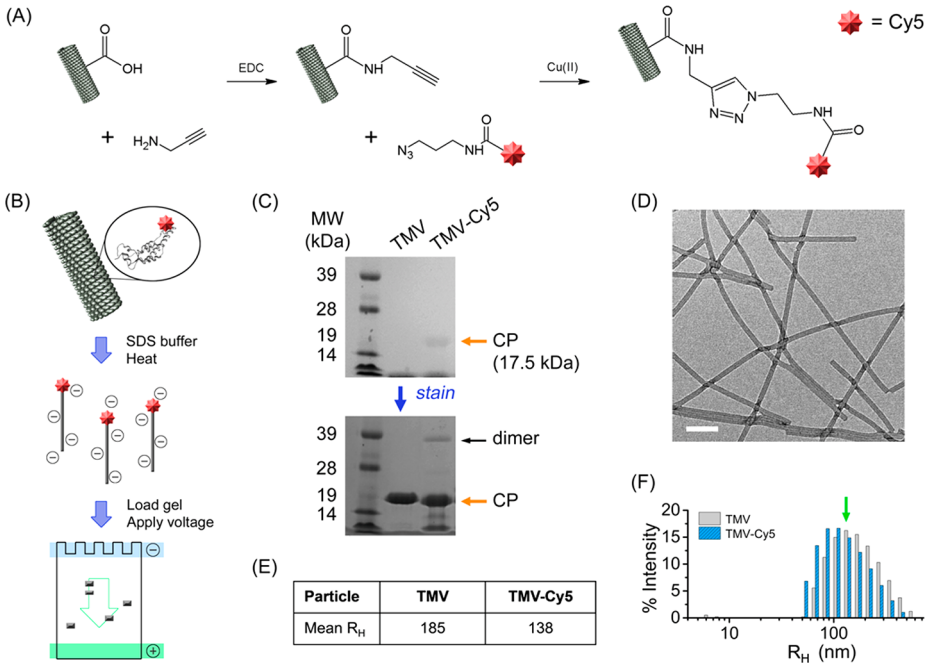


**Figure 2.** Fluorescent TMV-Cy5 synthesis and characterization. (A) Click reaction scheme for covalent attachment of Cy5 fluorophore to TMV coat proteins. (B) Schematic of TMV-Cy5 coat protein separation in SDS-PAGE. (C) SDS-PAGE of TMV-Cy5 before and after Coomassie staining, demonstrating covalent attachment of Cy5 to TMV (orange arrows). Low molecular weight protein bands are detectable in the TMV-Cy5 sample. We often observe these bands in chemically modified TMV samples. While these bands could be attributed to degraded TMV coat proteins, broken or free coat proteins are not detected by size exclusion chromatography and TEM imaging revealed intact particles. (D) TEM image demonstrating structural integrity of TMV-Cy5 (scale bar 100 nm). (E,F) DLS results showing reduced hydrodynamic radius ($R_H$) of TMV-Cy5 compared to unmodified TMV. Particle size distribution (shown in F) indicates high fraction of TMV-Cy5 remains at peak native particle size (green arrow), and the fraction of large particles (presumably aggregates) are reduced for TMV-Cy5.

resulting images were processed and analyzed using ImageJ 1.50i.[35]

**Cytotoxicity Assay.** Efficacy of TMV-cisPt was tested using Trevigen MTT assay and A2780 and OVCAR3, a model of PS and PR ovarian cancer, respectively. Each assay was performed twice and in triplicates and the normalized cell proliferation values averaged for each treatment concentration. Inhibitory concentration 50% ($IC_{50}$) was calculated from these averages. Cells were plated at $2 \times 10^3$ cells/well 1 day prior to the experiment. TMV-cisPt was freshly prepared on the day of each MTT experiment. Cells were treated with cisplatin concentrations in the range of 0.01−250 $\mu$M in triplicate for 24 h, then washed in PBS for 1 min to remove excess cisPt and TMV-cisPt (cisPt and TMV-cisPt not taken up by cells or expelled from cells as a function of drug transporters in PR cells). Then media was replenished and treatment continued for an additional 24 h for a total treatment time of 48 h. MTT reagent was added as per manufacturer's instructions. Reagent absorbance was determined using the Tecan infinite-M200 plate reader.

**$\gamma$-H2AX Foci Staining and Quantification.** A2780 and OVCAR3 cell lines were plated at $2.5 \times 10^4$ cells/well in triplicate over 1.5 mm thick coverslips in a 12-well plate 24 h prior to the experiment. Cells were treated for 24 h with equal volumes of PBS, cisPt in PBS, or TMV-cisPt in PBS with cisPt concentrations kept at 2 $\mu$M. Cells were then fixed in 4% (v/v) paraformaldehyde, permeabilized with 0.5% (v/v) Triton X-100 in PBS, and stained via immunofluorescence using 200 $\mu$L of mouse monoclonal antiphospho-histone H2AX antibody (1:500 dilution) and Alexa Fluor 488 antimouse secondary. Coverslips were then mounted onto slides using mounting medium with DAPI and imaged via a Leica scanning confocal microscope with 63× objective. Laser power and gain were kept constant for each sample and ten high powered fields were collected per sample. Cells with ten or more positive $\gamma$-H2AX foci in the nucleus were considered to have significant DNA double strand break (DSB) damage. Percentage of cells with significant DSB were quantified for all samples and statistically significant differences between groups was calculated by one-way ANOVA.

## RESULTS

**Synthesis and Characterization of TMV-cisPt.** TMV is comprised of 2130 identical coat proteins, with 4260 interior glutamic acid residues (Glu 97, 106) that can be deprotonated at basic pH and thus made available for electrostatic interactions with positively charged drug molecules, such as chemotherapies, photodynamic therapies, and nematicides, as we and others previously demonstrated.[25,26,31,36] Here, we used the aquated form of cisplatin, *cis*-$[Pt(NH_3)_2(H_2O)_2]^{2+}$ or cisPt+. Cisplatin is known to undergo nucleophilic substitution in water to form cisPt+;[37] this product can be reliably obtained from reaction with silver nitrate.[31] This activated form of cisplatin is biologically more active in forming DNA cross-links and is naturally formed in the intracellular space following cisplatin uptake, however, its presence in the bloodstream is not favored due to the relatively high concentration of reducing chloride ions.[38]

Loading into TMV was tested in parallel with freshly suspended cisPt and its aqueous form, cisPt+ (Figure 1A). CisPt/cisPt+ was mixed in solution with TMV; pH and molar excess of cisPt(+)-to-TMV were parameters tested to optimize the loading procedure. The reaction mix was incubated for 2 h;


DOI: 10.1021/acs.molpharmaceut.7b00466
Mol. Pharmaceutics XXXX, XXX, XXX−XXX

TMV-cisPt was then purified by ultracentrifugation to remove unbound, excess drug molecules. A schematic cross-section of TMV loaded with cisplatin is shown in Figure 1B, and the expected predominant chemical structure is shown based on previous studies with phenanthriplatin, a derivative of cisplatin with analogous structure.[26] Purified TMV-cisPt were found to remain structurally sound, as confirmed by transmission electron microscopy (Figure 1C).

The resulting molar ratio of cisplatin (MW 304.55 g/mol) to TMV (MW $3.94 \times 10^7$ g/mol) was determined by measuring cisplatin content with graphite furnace atomic absorption spectrometry (GF-AAS) and TMV concentration with UV−visible spectrophotometry (UV−vis) and TMV-specific extinction coefficient (3.0 $mg^{-1}$ mL $cm^{-1}$, 260 nm), with results summarized in Figure 1D.[33] Data indicate that neutral cisPt does not interact with TMV within 2 h; at 20k equiv, cisPt has little to no loading (12 ± 9 mol cisPt:TMV) while cisPt+ achieved a near 1:1 ratio of drug:coat protein (1,813 ± 128 mol cisPt:TMV; each TMV particle consists of 2130 identical copies of a coat protein) (Figure 1E).

Optimal cisPt+ loading conditions were determined by performing this reaction using a panel of cisPt+ molar equivalents and pH values. All loading results are shown in Figure 1D. Increased molar excess resulted in increased loading of cisPt+, with 5k, 10k, and 20k equivalents achieving drug:TMV loading ratios of 665 ± 49, 1,351 ± 141, and 1813 ± 128 mol cisPt:TMV, respectively (Figure 1E). No significant difference in loading was observed with various buffer pH, but pH 7.8 was chosen due to improved loading uniformity (Figure 1F). From these data, we determined the optimal procedure of TMV-cisPt loading was a reaction with 20k molar excess cisPt+ at pH 7.8.

To evaluate the profile of cisplatin release from TMV, TMV-cisPt was dialyzed against PBS at physiological conditions (pH 7.4) and pH-adjusted PBS to simulate acidic tumor microenvironment (pH 5.4). Fractions of TMV-cisPt were collected over the course of 72 h, and remaining cisplatin content per TMV at each time point was measured using GF-AAS and UV−vis as described above. The dialysis results demonstrated a biphasic release profile with a fast half-life ($t_1$) of 0.93 and 1.06 h and slow half-life ($t_2$) of 13.85 and 12.91 h at physiological and acidic pH, respectively. No significant differences were observed studying the release rates at neutral vs acidic pH; at either pH 7.4 and 5.4, 50% of the cisPt-load was released from its TMV carrier after approximately 5 h. Toward the end of the 72 h dialysis period, both curves approach asymptotic values with 30−40% of the drug cargo remaining associated with the TMV carrier (Figure 1G), suggesting that a fraction of encapsulated cisPt may be stably bound to the TMV interior.

**Cellular Uptake of TMV.** Uptake of TMV in A2780 and OVCAR3 cells was analyzed using flow cytometry and TMV fluorescently labeled with Cy5 (termed TMV-Cy5) using click chemistry (Figure 2A). Because the exterior surfaces of both TMV-cisPt and TMV-Cy5 were unmodified, the cellular interactions with TMV-Cy5 were expected to be representative of TMV-cisPt. SDS-PAGE confirmed covalent attachment of Cy5 to TMV coat proteins (Figure 2B). Before staining of the gel, a Cy5 band visible in white light was observed to colocalize with the TMV coat protein (CP) band at 17.5 kDa, which was visible after coomassie staining (Figure 2C). TMV-Cy5 integrity was confirmed by TEM (Figure 2D) and DLS with reference to native TMV (Figure 2E,F). Mean hydrodynamic radii ($R_H$) of TMV and TMV-Cy5 were determined with DLS to be 185 and 138 nm, respectively (Figure 2E); the particle size distribution shows that a high fraction of particles maintained the peak radius of native TMV (Figure 2F), revealing no significant difference between the samples. The reduced fraction of particles with radius >200 nm in TMV-Cy5 indicates that fewer large aggregates are present in TMV-Cy5 vs native TMV, most likely due to the extensive purification of the chemically modified TMV-Cy5.

Flow cytometry analysis of A2780 and OVCAR3 epithelial ovarian cancer cells postexposure to TMV demonstrated that TMV interacts with both cell lines (Figure 3A). Data indicate

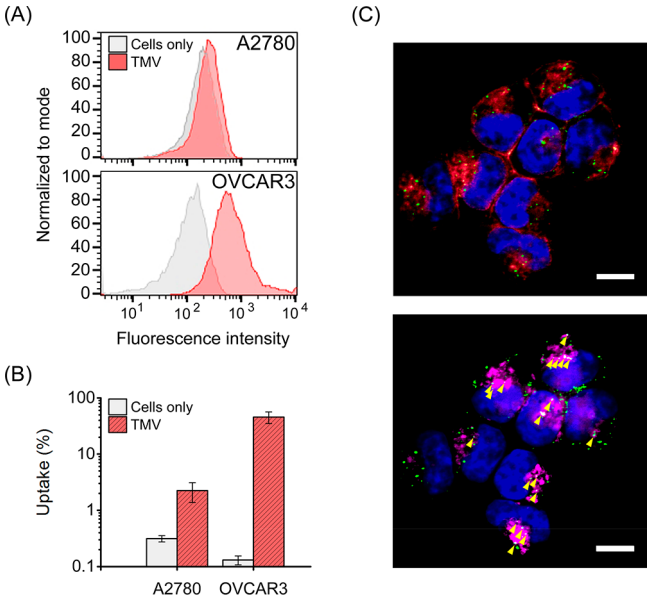


**Figure 3.** Cellular interactions with TMV. (A) FACS histograms showing cell-TMV interactions in A2780 and OVCAR3 cells, with more pronounced shift in fluorescence intensity between control cells and TMV-treated cells in OVCAR3. Experiments were performed in triplicate and repeated once; data shown are representative data from single experiments. (B) FACS analysis of cell-TMV interactions shown as percent of cell population positive for Cy5 fluorescence, indicating enhanced TMV interactions with OVCAR3. Experiments were performed in triplicate and repeated once; data shown are mean ± SD from triplicate samples. 10 000 events were recorded, and data was analyzed using FlowJo software 10.2. (C) Representative fluorescent images indicate internalization of TMV (green) in A2780 cells with TMV-endolysosome colocalization shown in white and indicated by yellow arrowheads (scale bar 10 $\mu$m). Cells were incubated for 24 h with $2.5 \times 10^6$ particles/cell and stained for TMV (green), cell membrane (red, shown in the top panel), endolysosomes (magenta, shown in the bottom panel), and nuclei (blue). TMV gives a punctate signal indicating localization within vesicular compartments; partial colocalization with the endolysosomal marker LAMP-1 is observed.

more pronounced interactions of TMV with OVCAR3 vs A2780 cells. While only 3% of A2780 cells showed positive for TMV, 47% of OVCAR3 cells had internalized TMV at the given concentration ($1 \times 10^5$ particles/cell) and 15 h incubation time (Figure 3B). The differences in cell uptake may be due to distinct metabolic rates of the two cell lines. Given the low uptake rates in the A2780 cell line as indicated by FACS, to verify TMV uptake in A2780 we also performed fluorescence microscopy experiments using this cell line; imaging studies confirmed that TMV is indeed internalized into these cells, with a punctate signal indicating localization


DOI: 10.1021/acs.molpharmaceut.7b00466
Mol. Pharmaceutics XXXX, XXX, XXX−XXX

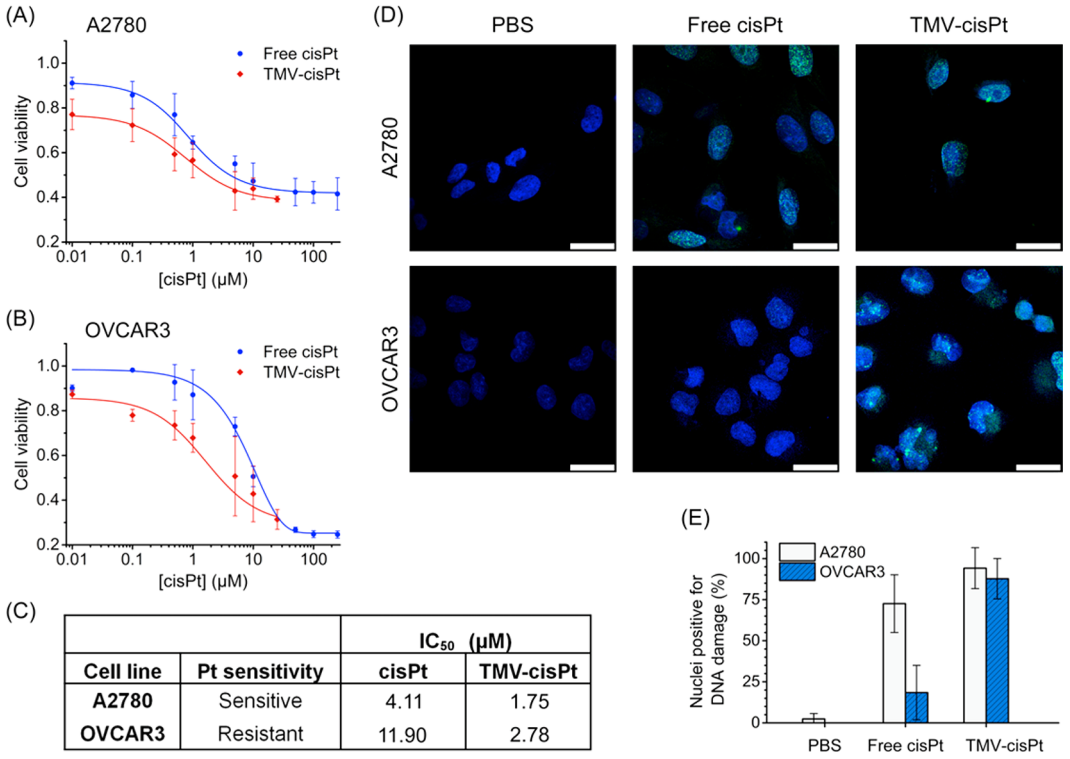


(C)

| | | $IC_{50}$ (μM) | |
|---|---|---|---|
| Cell line | Pt sensitivity | cisPt | TMV-cisPt |
| A2780 | Sensitive | 4.11 | 1.75 |
| OVCAR3 | Resistant | 11.90 | 2.78 |

**Figure 4.** TMV-cisPt cytotoxicity and DNA damage. (A) Cells were treated with a range of drug concentrations in PBS. After 24 h of treatment, cells were washed in PBS and treatment continued for a total of 48 h. MTT assay performed on Pt-sensitive A2780 cells, indicating TMV-cisPt has greater efficacy at low concentrations than free cisPt. (B) MTT assay performed on Pt-resistant OVCAR3 cells, demonstrating superior treatment efficacy of TMV-cisPt at all tested concentrations of cisPt. (C) $IC_{50}$ values for free cisPt and TMV-cisPt as calculated from MTT assay results. (D) Representative confocal images of A2780 and OVCAR3 cells reveal H2AX phosphorylation (γ-H2AX, green) in nuclei (blue) as a result of treatment with TMV-cisPt compared to free cisPt and PBS (scale bar 25 μm). Increased γ-H2AX phosphorylation in OVCAR3 cells treated with TMV-cisPt indicates increased efficacy of TMV-cisPt over free cisPt for inducing DNA damage in PR cells at low dosage. Cells were incubated for 24 h with equal volumes of PBS, cisPt, or TMV-cisPt with cisPt concentrations of 2 μM and stained for γ-H2AX (green) and nuclei (blue). (E) Quantification of DNA double strand breakage (DSB) shown as percent of nuclei positive for γ-H2AX foci (mean ± SD), averaged from a total of ten fields per sample (≥10 γ-H2AX foci/nucleus indicated positive for DSB). All treatment groups for each cell line were determined by one-way ANOVA to be statistically significant ($p < 0.05$) compared to other treatments as well as to PBS control.

within vesicular compartments. Partial colocalization with the LAMP-1 endolysosomal marker is observed, presumably following phagosome−lysosome fusion into mature endolysosomes (Figure 3C).

**TMV-cisPt Cytotoxicity and DNA Damage.** The anticancer efficacy of TMV-cisPt was tested by MTT cytotoxicity assay in parallel with free cisPt against PS and PR epithelial ovarian cancer cell lines. A2780 was chosen as a representative model for untreated PS disease based on its derivation from an untreated ovarian tumor, as well as its widespread acceptance as a PS cell line,[40−42] and OVCAR3 was chosen as a representative model for PR disease based on its origin from refractory ovarian cancer previously treated with cisplatin.[40,41] The $IC_{50}$ results indicate that TMV-cisPt outperforms free cisplatin in the PS model, with an even more significant improvement in the PR model (Figure 4A,B). While the $IC_{50}$ values for free cisplatin in A2780 and OVCAR3 were 4.11 μM and 11.90 μM, respectively, TMV-cisPt demonstrated enhanced efficacy, with respective $IC_{50}$ values of 1.75 μM and 2.78 μM (Figure 4C). Although the cytotoxicity of cisplatin plateaus at 50 μM in OVCAR3 cells, TMV-cisPt shows more complete cell killing at lower concentrations.

To investigate the mechanism of enhanced cytotoxicity in PR cells, the DNA double strand break (DSB) damage was quantified via confocal imaging of phosphorylated histone H2AX (γ-H2AX) foci after treatment of A2780 and OVCAR3 cells with 2 μM free cisPt or TMV-cisPt for 24 h. Ten fields were imaged per sample, and all nuclei with 10 or more γ-H2AX foci were selected as positive for DSB. Representative images are shown (Figure 4D). PBS-treated controls showed little to no DSB in either A2780 (2.4 ± 3.3%) or OVCAR3 (0 ± 0%). All treatment groups resulted in significant DSB compared to controls ($p < 0.05$), as analyzed by one-way ANOVA, with f-statistics $2.272 \times 10^{-15}$ and $2.026 \times 10^{-15}$ for A2780 and OVCAR3, respectively (Figure 4E). DSB was moderately, but significantly ($p = 0.0065$), increased in PS cells (A2780) by treatment with TMV-cisPt (94.2 ± 12.5%) compared to free cisPt (72.6 ± 17.6%). More notably, in PR cells (OVCAR3), nuclei positive for DSB were dramatically increased by treatment with TMV-cisPt (87.7 ± 12.3%) compared to free cisPt (18.5 ± 16.6%) ($p = 2.8 \times 10^{-7}$) (Figure 4E). These results indicate that the efficacy of cisPt treatment for inducing DNA damage is enhanced at low dosage, especially in PR cells, by encapsulation in TMV.

## DISCUSSION

Treatment of ovarian cancer with platinum-based chemotherapeutics consistently leads to development of platinum resistance over time, but because of high initial efficacy of


DOI: 10.1021/acs.molpharmaceut.7b00466
Mol. Pharmaceutics XXXX, XXX, XXX−XXX

platinum therapy, combined with inferiority of many alternative treatment candidates, platinum drugs, such as cisplatin, remain the standard of care for ovarian cancer therapy.[2,43] In some cases, resistance may be overcome by dose escalation, but this approach endangers patient quality of life due to amplified systemic toxicity.[5,41] This work presents TMV-cisPt as a substitute for dose escalation in the treatment of patients presenting platinum-resistant ovarian cancer. We have developed a charge-driven protocol for loading of cisplatin into the interior channel of the tobacco mosaic virus (TMV), examined TMV-assisted cisplatin delivery to PS and PR ovarian cancer cell lines, and demonstrated the superiority of this TMV-cisPt system for treatment of PS and PR ovarian cancer cells *in vitro*.

A simple and reliable protocol was developed allowing for efficient cisplatin loading into TMV achieving almost 1:1 cisplatin:TMV coat protein ratios. Like the classic CuAAC click reaction we used to bind a fluorophore to the interior glutamic acids of TMV-Cy5, the reaction between TMV and cisPt shares the characteristics that were originally described by Sharpless and Finn to make click reactions reliable and scalable for clinical development and manufacture;[32] the TMV-cisPt reaction has high yields in simple, aqueous reaction conditions, and the AgCl byproduct and final reaction product are easily purified by centrifugation without the need for chromatography. Also consistent with click chemistry, this reaction demonstrates some degree of modularity. The reaction with cisPt is consistent with analogous drug molecules investigated in previous studies: for example, phenanthriplatin (phenPt), a cisplatin analogue and novel drug candidate, was loaded at similar rates with 2000 ± 200 phenPt:TMV, and was shown to be highly selective for the interior channel.[26] Because of the analogous structures of cisPt and phenPt, we anticipate that cisPt is likewise restricted to interior loading in these reaction conditions.

Similar reactions with the interior glutamic acid residues of TMV have also demonstrated wide applicability for the loading of other small molecules. In another example, we demonstrated encapsulation of a cationic photosensitizer, 5-(4-ethynylphenyl)-10,15,20-tris(4-methylpyridin-100 4-ium-1-yl)porphyrin-zinc(II) triiodide (Zn-EpPor), for photodynamic therapy applications; here loading efficiency was at 900 ± 135 Zn-EpPor:TMV.[25] The difference in charge between the platinum drugs and Zn-EpPor could the defining factor affecting drug loading efficiency; the platinum drugs carry 2+ charges while Zn-EpPor carries a 3+ charge, which is hypothesized to result in greater charge neutralization of the TMV particle and thus may lessen the total capacity for loading Zn-EpPor. Most recently we demonstrated that these protocols can also be extended to tobacco mild green mosaic virus (TMGMV), a close cousin of TMV. Here we demonstrated loading of nematicides for agriculture applications.[36] Together these studies suggest that the loading of therapeutic molecules into TMV's interior channel making use of charge-driven "click" protocol is a reliable mechanism and may be extended to a wide variety of molecules.

The mechanism of cisplatin loading into the TMV interior channel is likely coordination bonding, which has been previously demonstrated for effective loading of TMV with platinum-based drug molecules.[26] The results of dialysis of TMV-cisPt support this hypothesis. The biphasic release profile demonstrates an initial burst release between 0 and 5 h followed by a slower release phase with a more prolonged half-life. The burst release may represent cisplatin molecules that are loaded via noncovalent electrostatic attractions, and the second release phase likely represents the fraction of molecules bonded to the TMV coat proteins, approaching an asymptotic value of cisplatin content at which the binding of cisplatin is highly stable.

Although complete release of cisplatin is not observed at either pH tested, this *in vitro* behavior may not realistically mimic the *in vivo* release. Our data show that when TMV is taken up by cancer cells (here A2780), the TMV appears to be localized within endocytic vesicles scattered within the cell. This phenomenon is consistent with the formation of phagosomes at the cell periphery which is followed by microtubule-mediated trafficking toward the nucleus, where the majority of LAMP-1 positive lysosomes reside.[44] Presumably following phagosome−lysosome fusion into mature endolysosomes,[44] TMV is seen to colocalize at least in part with these endolysosomal compartments, and this is consistent with our previous observations using various cell lines.[26,33] The acidic pH and proteolytic activity of the endolysosomal compartment is expected to further drive cisPt release through protonation of TMV's carboxylates (due to the acidic pH) and protein degradation of the TMV protein carrier (based on proteolytic activity).

pH-dependent drug release has been a common topic of research for cancer therapy, including ovarian cancer, due to the acidic intratumoral microenvironment that would stimulate site-specific release.[45,46] However, since the hypothesized mechanisms for platinum resistance in ovarian cancer include upregulation of cisplatin efflux,[7] release of cisplatin in or around the cancerous tissue may not improve efficacy significantly. Instead, a method to increase uptake and retention of drug molecules inside cancer cells would be more promising for resensitization of PR disease, and our results suggest that TMV-cisPt has potential in this area. Cell studies demonstrate TMV uptake in both cell lines, with significantly more profound TMV uptake in the OVCAR3 vs A2780 cell line. When compared to the cell killing efficacy, it is suggested that the enhanced OVCAR3 cell interactions may contribute to lower $IC_{50}$ values restoring cisplatin sensitivity in this PR cell model. MTT assay provided $IC_{50}$ values for cisPt and TMV-cisPt, respectively: 4.11 and 1.75 in A2780, and 11.90 and 2.78 $\mu$M in OVCAR3, demonstrating a reduction in $IC_{50}$ of more than 75% in platinum-resistant OVCAR3 by treatment with TMV-cisPt. This is in stark contrast to previous efforts using liposomal formulations of cisplatin: Lipoplatin exhibited reduced efficacy when compared to cisplatin in the F98 glioma cell line, potentially due to a nonfavorable intracellular distribution of cisplatin following cellular uptake.[47] From these experiments, it can be deduced that the enhanced efficacy of TMV-cisPt in PS and PR cells occurs as a result of either increased rate of drug uptake, increased drug retention, or increased DNA damage resulting from encapsulation of cisplatin in the TMV nanocarrier.

To address the latter, we have investigated this phenomenon of cisplatin resensitization by examining DSB in DNA as a result of treatment of PS and PR ovarian cancer cells with free and TMV-encapsulated cisplatin. An established indicator of lethal DSB is a high incidence of phosphorylated histone $\gamma$-H2AX foci remaining in cell nuclei 24 h after treatment with cisplatin.[48] Increased presence of $\gamma$-H2AX foci in nuclei after 24 h of treatment with equal concentrations of TMV-cisPt vs free cisPt revealed greater occurrence of DSB and subsequent cell


DOI: 10.1021/acs.molpharmaceut.7b00466
*Mol. Pharmaceutics* XXXX, XXX, XXX−XXX

killing by treatment with TMV-encapsulated cisplatin in both A2780 (PS) and OVCAR3 (PR) cells. Remarkably, percentages of PR cells positive for lethal DSB were increased from 18.5 ± 16.6% with free cisPt treatment to 88.7 ± 12.3% with TMV-cisPt. This study supports the results of our MTT experiments which indicated a reduced effective dosage for TMV-cisPt compared to free cisPt, with markedly improved cell killing by TMV-cisPt in PR cells. Therefore, we conclude that delivery of cisplatin via TMV as a nanocarrier is capable of circumventing mechanisms of resistance in PR cells and restoring efficacy of cisplatin treatment at low concentrations.

The use of nanoparticles for delivery of cisplatin is not a novel concept; this strategy has gained popularity in recent years due to the probability that this approach would reduce off-target toxic side effects. Attempted nanocarrier systems for cisplatin include liposomes, polymeric carriers, and metallic particles, among others.[12] None of these formulations, however, have yet proven to provide clinically relevant improvement over free cisplatin in PR ovarian cancer, and some nanoparticles tested in other cancer types have demonstrated improved efficacy over free drug *in vivo*.

TMV provides an alternative to the contemporary explored synthetic platforms. While its clinical utility is yet to be demonstrated, the biology-derived material possesses intriguing properties for *in vivo* medical applications: TMV is biocompatible and tolerated *in vivo* at doses up to 50 mg/kg.[22] While uncoated TMV is immunogenic, stealth and camouflage coatings have been established to reduce immune surveillance and antibody recognition.[49−51] Another benefit is the highly controlled and tunable structure and surface chemistry allowing the assembly and synthesis of monodisperse nanomaterials.[52] Native TMV is comprised of 2130 identical coat proteins with chemically available amino acid residues on its interior and exterior surfaces.[49,53] Here we made use of the Glu acid functionality lining TMV's interior channel. We developed a simple "click" reaction between interior glutamic acids and positively charged cisplatin yielding ∼1:1 ratio of cisplatin:TMV coat protein, the reaction is simple, performed by in-solution mixing of cisplatin and TMV in aqueous buffer; the TMV-cisPt product is purified in one step by ultracentrifugation. Further modifications could be carried out and surface functional groups, such as stealth/camouflage coatings or ligands for targeting strategies, could be introduced to impart new functionality.

Other advantageous properties of TMV will also aid in translatability of experimental results to clinical effects. Moving forward to large-scale production, commercially viable nanoparticle systems must be obtained using scalable manufacturing that is cost-effective and environmentally sustainable. Comparing manufacturability of TMV to synthetic nanoparticles, TMV has greater ease of production and decreased environmental hazard. Propagation of nanoparticles in plant systems is capable of high yield and rapid production at relatively low cost that will fulfill the high demand required for biomedical applications.[54] Further, our protocol for TMV production is more environmentally safe than typical protocols for lipid or polymeric nanoparticle synthesis. Chemical synthesis processes often use DCM (dichloromethane) or DMSO (dimethyl sulfoxide) which may be hazardous to the environment on a large scale.[55] Although "green" synthesis methods are currently being explored for synthetic nanoparticle production, these methods can result in reduced yield and are unfit for large scale production at this time.[55] Accordingly, plant virus-based nanoparticles are more favorable than synthetic nanoparticles for large-scale medical applications.

## CONCLUSIONS

We developed a simple and reliable "click" chemistry protocol yielding TMV-cisPt formulations shown to be effective in the delivery of cisplatin to ovarian cancer cells. Most importantly our data indicate that platinum delivery by TMV has potential to restore efficacy in platinum-resistant disease. Enhanced treatment response in patients presenting PR ovarian cancers is especially urgent since the current response rate in these patients is only 10−15% with a median progression-free survival of merely 3−4 months.[5] Based on cytotoxicity studies performed on established models of PS and PR ovarian cancers, our plant virus-based nanocarrier has shown promise *in vitro* for reducing effective cisplatin dosage in first-line treatment of ovarian cancer as well as for increasing the potency of cisplatin treatment in refractory disease. Our studies highlight the potential of TMV as a drug carrier, future studies will provide insights into the translational potential of the plant virus-based nanotechnology.

## AUTHOR INFORMATION

### Corresponding Author

*E-mail: nicole.steinmetz@case.edu.

### ORCID

Nicole F. Steinmetz: 0000-0002-0130-0481

### Author Contributions

C.E.F. performed the synthesis and characterization of TMV-cisPt and TMV-Cy5, analyzed cell uptake and efficacy. A.E.C. performed fluorescence microscopy studies and helped with the characterization of the TMV-cisPt construct. R.B.P. performed DNA damage experiments. N.F.S. conceived and oversaw the entire study. C.E.F. and N.F.S. wrote the manuscript. All authors read, edited, and approved the manuscript.

### Notes

The authors declare no competing financial interest.

## ACKNOWLEDGMENTS

This work was funded in part by a grant from the National Science Foundation, CMMI-1333651 to N.F.S. Paul L. Chariou is thanked for assistance with TEM imaging.

## REFERENCES

(1) Jayson, G. C.; Kohn, E. C.; Kitchener, H. C.; Ledermann, J. A. Ovarian cancer. *Lancet* **2014**, *384* (9951), 1376−1388.

(2) Ganghadaran, S. G. D. Management of Platinum Resistant - Refractory Ovarian Cancer: A Short Review. *Journal of Cancer Research and Treatment* **2016**, *4* (2), 32−36.

(3) Meng, E.; Long, B.; Sullivan, P.; McClellan, S.; Finan, M. A.; Reed, E.; Shevde, L.; Rocconi, R. P. CD44+/CD24- ovarian cancer cells demonstrate cancer stem cell properties and correlate to survival. *Clin. Exp. Metastasis* **2012**, *29* (8), 939−48.

(4) Liu, J.; Matulonis, U. A. New Strategies in Ovarian Cancer: Translating the Molecular Complexity of Ovarian Cancer into Treatment Advances. *Clin. Cancer Res.* **2014**, *20* (20), 5150.

(5) Webber, K.; Friedlander, M. Chemotherapy for epithelial ovarian, fallopian tube and primary peritoneal cancer. *Best Practice & Research Clinical Obstetrics & Gynaecology* **2017**, *41*, 126.

(6) Helm, C. W.; States, J. C. Enhancing the efficacy of cisplatin in ovarian cancer treatment − could arsenic have a role. *J. Ovarian Res.* **2009**, *2* (1), 2.



DOI: 10.1021/acs.molpharmaceut.7b00466
*Mol. Pharmaceutics* XXXX, XXX, XXX−XXX

(7) Stewart, D. J. Mechanisms of resistance to cisplatin and carboplatin. *Critical Reviews in Oncology/Hematology* **2007**, *63* (1), 12−31.
(8) Herzog, T. J.; Armstrong, D. K. First-line chemotherapy for advanced (stage III or IV) epithelial ovarian, fallopian tubal, and peritoneal cancer. *UpToDate* **2016**.
(9) Stewart, L.; Chemotherapy for advanced ovarian cancer. *Cochrane Database of Systematic Reviews* **1999**, *(1)*.10.1002/14651858.CD001418
(10) Alberts, D. S. Carboplatin versus cisplatin in ovarian cancer. *Semin Oncol* **1995**, *22*, 88−90.
(11) Markman, M.; Olawaiye, A. B. Intraperitoneal chemotherapy for treatment of ovarian cancer. *UpToDate* **2016**.
(12) Duan, X.; He, C.; Kron, S. J.; Lin, W. Nanoparticle formulations of cisplatin for cancer therapy. *Wiley Interdisciplinary Reviews: Nanomedicine and Nanobiotechnology* **2016**, *8* (5), 776−791.
(13) Wong, B. S.; Yoong, S. L.; Jagusiak, A.; Panczyk, T.; Ho, H. K.; Ang, W. H.; Pastorin, G. Carbon nanotubes for delivery of small molecule drugs. *Adv. Drug Delivery Rev.* **2013**, *65* (15), 1964−2015.
(14) Liang, X.-J.; Meng, H.; Wang, Y.; He, H.; Meng, J.; Lu, J.; Wang, P. C.; Zhao, Y.; Gao, X.; Sun, B.; Chen, C.; Xing, G.; Shen, D.; Gottesman, M. M.; Wu, Y.; Yin, J.-j.; Jia, L. Metallofullerene nanoparticles circumvent tumor resistance to cisplatin by reactivating endocytosis. *Proc. Natl. Acad. Sci. U. S. A.* **2010**, *107* (16), 7449−7454.
(15) Ren, F.; Shen, J.; Shi, H.; Hornicek, F. J.; Kan, Q.; Duan, Z. Novel mechanisms and approaches to overcome multidrug resistance in the treatment of ovarian cancer. *Biochim. Biophys. Acta, Rev. Cancer* **2016**, *1866* (2), 266−275.
(16) Wen, A. M.; Steinmetz, N. F. Design of virus-based nanomaterials for medicine, biotechnology, and energy. *Chem. Soc. Rev.* **2016**, *45* (15), 4074−4126.
(17) Giacca, M.; Zacchigna, S. Virus-mediated gene delivery for human gene therapy. *J. Controlled Release* **2012**, *161* (2), 377−388.
(18) Lee, C. S.; Bishop, E. S.; Zhang, R.; Yu, X.; Farina, E. M.; Yan, S.; Zhao, C.; Zeng, Z.; Shu, Y.; Wu, X.; Lei, J.; Li, Y.; Zhang, W.; Yang, C.; Wu, K.; Wu, Y.; Ho, S.; Athiviraham, A.; Lee, M. J.; Wolf, J. M.; Reid, R. R.; He, T.-C. Adenovirus-mediated gene delivery: Potential applications for gene and cell-based therapies in the new era of personalized medicine. *Genes & Diseases* **2017**, *4* (2), 43−63.
(19) Lico, C.; Schoubben, A.; Baschieri, S.; Blasi, P.; Santi, L. Nanoparticles in Biomedicine: New Insights from Plant Viruses. *Curr. Med. Chem.* **2013**, *20* (28), 3471−3487.
(20) Farr, R.; Choi, D. S.; Lee, S.-W. Phage-based nanomaterials for biomedical applications. *Acta Biomater.* **2014**, *10* (4), 1741−1750.
(21) Czapar, A. E.; Steinmetz, N. F. Plant viruses and bacteriophages for drug delivery in medicine and biotechnology. *Curr. Opin. Chem. Biol.* **2017**, *38*, 108−116.
(22) Bruckman, M. A.; Randolph, L. N.; VanMeter, A.; Hern, S.; Shoffstall, A. J.; Taurog, R. E.; Steinmetz, N. F. Biodistribution, pharmacokinetics, and blood compatibility of native and PEGylated tobacco mosaic virus nano-rods and -spheres in mice. *Virology* **2014**, *449*, 163−173.
(23) Koudelka, K. J.; Pitek, A. S.; Manchester, M.; Steinmetz, N. F. Virus-Based Nanoparticles as Versatile Nanomachines. *Annu. Rev. Virol.* **2015**, *2* (1), 379−401.
(24) Bruckman, M. A.; Czapar, A. E.; VanMeter, A.; Randolph, L. N.; Steinmetz, N. F. Tobacco mosaic virus-based protein nanoparticles and nanorods for chemotherapy delivery targeting breast cancer. *J. Controlled Release* **2016**, *231*, 103−113.
(25) Lee, K. L.; Carpenter, B. L.; Wen, A. M.; Ghiladi, R. A.; Steinmetz, N. F. High Aspect Ratio Nanotubes Formed by Tobacco Mosaic Virus for Delivery of Photodynamic Agents Targeting Melanoma. *ACS Biomater. Sci. Eng.* **2016**, *2* (5), 838−844.
(26) Czapar, A. E.; Zheng, Y.-R.; Riddell, I. A.; Shukla, S.; Awuah, S. G.; Lippard, S. J.; Steinmetz, N. F. Tobacco Mosaic Virus Delivery of Phenanthriplatin for Cancer therapy. *ACS Nano* **2016**, *10* (4), 4119−4126.
(27) Le, D. H. T.; Lee, K. L.; Shukla, S.; Commandeur, U.; Steinmetz, N. F. Potato virus X, a filamentous plant viral nanoparticle for doxorubicin delivery in cancer therapy. *Nanoscale* **2017**, *9* (6), 2348−2357.
(28) Kernan, D. L.; Wen, A. M.; Pitek, A. S.; Steinmetz, N. F. Delivery of chemotherapeutic vcMMAE using tobacco mosaic virus nanoparticles. *Exp. Biol. Med.* **2017**, *242* (14), 1405−1411.
(29) Hu, H.; Zhang, Y.; Shukla, S.; Gu, Y.; Yu, X.; Steinmetz, N. F. Dysprosium-Modified Tobacco Mosaic Virus Nanoparticles for Ultra-High-Field Magnetic Resonance and Near-Infrared Fluorescence Imaging of Prostate Cancer. *ACS Nano* **2017**, DOI: 10.1021/acsnano.7b04472.
(30) Bruckman, M. A.; Steinmetz, N. F. Chemical Modification of the Inner and Outer Surfaces of Tobacco Mosaic Virus (TMV). In *Virus Hybrids as Nanomaterials: Methods and Protocols*; Lin, B., Ratna, B., Eds.; Humana Press: Totowa, NJ, 2014; pp 173−185.
(31) Poklar, N.; Pilch, D. S.; Lippard, S. J.; Redding, E. A.; Dunham, S. U.; Breslauer, K. J. Influence of cisplatin intrastrand crosslinking on the conformation, thermal stability, and energetics of a 20-mer DNA duplex. *Proc. Natl. Acad. Sci. U. S. A.* **1996**, *93* (15), 7606−7611.
(32) Kolb, H. C.; Finn, M. G.; Sharpless, K. B. Click Chemistry: Diverse Chemical Function from a Few Good Reactions. *Angew. Chem., Int. Ed.* **2001**, *40* (11), 2004−2021.
(33) Wen, A. M.; Infusino, M.; De Luca, A.; Kernan, D. L.; Czapar, A. E.; Strangi, G.; Steinmetz, N. F. Interface of Physics and Biology: Engineering Virus-Based Nanoparticles for Biophotonics. *Bioconjugate Chem.* **2015**, *26* (1), 51−62.
(34) Shukla, S.; Eber, F. J.; Nagarajan, A. S.; DiFranco, N. A.; Schmidt, N.; Wen, A. M.; Eiben, S.; Twyman, R. M.; Wege, C.; Steinmetz, N. F. The Impact of Aspect Ratio on the Biodistribution and Tumor Homing of Rigid Soft-Matter Nanorods. *Adv. Healthcare Mater.* **2015**, *4* (6), 874−882.
(35) Rasband, W. S. *ImageJ*; U.S. National Institutes of Health: Bethesda, MD, USA, 1997−2016.
(36) Chariou, P. L.; Steinmetz, N. F. Delivery of Pesticides to Plant Parasitic Nematodes using Tobacco Mild Green Mosaic Virus as a Nanocarrier. *ACS Nano* **2017**, *11*, 4719.
(37) Long, D. F.; Repta, A. J.; Sternson, L. A. The reactivity of cisplatin in plasma. Implications for sample handling in pharmacokinetic studies. *Int. J. Pharm.* **1980**, *6* (2), 167−173.
(38) Jones, C.; Thornback, J. *Medicinal Applications of Coordination Chemistry*; Royal Society of Chemistry, 2007.
(39) Pettersen, E. F.; Goddard, T. D.; Huang, C. C.; Couch, G. S.; Greenblatt, D. M.; Meng, E. C.; Ferrin, T. E. UCSF Chimera–a visualization system for exploratory research and analysis. *J. Comput. Chem.* **2004**, *25* (13), 1605−12.
(40) Godwin, A. K.; Meister, A.; O'Dwyer, P. J.; Huang, C. S.; Hamilton, T. C.; Anderson, M. E. High resistance to cisplatin in human ovarian cancer cell lines is associated with marked increase of glutathione synthesis. *Proc. Natl. Acad. Sci. U. S. A.* **1992**, *89* (7), 3070−4.
(41) Perez, R. P.; Perez, K. M.; Handel, L. M.; Hamilton, T. C. In vitro interactions between platinum analogues in human ovarian-carcinoma cell lines. *Cancer Chemother. Pharmacol.* **1992**, *29* (6), 430−434.
(42) Kakar, S. S.; Ratajczak, M. Z.; Powell, K. S.; Moghadamfalahi, M.; Miller, D. M.; Batra, S. K.; Singh, S. K. Alone and in Combination with Cisplatin Suppresses Growth and Metastasis of Ovarian Cancer by Targeting Putative Cancer Stem Cells. *PLoS One* **2014**, *9* (9), e107596.
(43) Bell-McGuinn, K.; Konner, J.; Tew, W.; Spriggs, D. R. New drugs for ovarian cancer. *Annals of Oncology* **2011**, *22* (8), viii77−viii82.
(44) Huynh, K. K.; Eskelinen, E. L.; Scott, C. C.; Malevanets, A.; Saftig, P.; Grinstein, S. LAMP proteins are required for fusion of lysosomes with phagosomes. *EMBO J.* **2007**, *26* (2), 313−324.
(45) Heinrich, A.-K.; Lucas, H.; Schindler, L.; Chytil, P.; Etrych, T.; Mäder, K.; Mueller, T. Improved Tumor-Specific Drug Accumulation by Polymer Therapeutics with pH-Sensitive Drug Release Overcomes Chemotherapy Resistance. *Mol. Cancer Ther.* **2016**, *15* (5), 998−1007.


DOI: 10.1021/acs.molpharmaceut.7b00466
*Mol. Pharmaceutics* XXXX, XXX, XXX−XXX

(46) Li, H.-J.; Du, J.-Z.; Du, X.-J.; Xu, C.-F.; Sun, C.-Y.; Wang, H.-X.; Cao, Z.-T.; Yang, X.-Z.; Zhu, Y.-H.; Nie, S.; Wang, J. Stimuli-responsive clustered nanoparticles for improved tumor penetration and therapeutic efficacy. *Proc. Natl. Acad. Sci. U. S. A.* **2016**, *113* (15), 4164−4169.
(47) Charest, G.; Paquette, B.; Fortin, D.; Mathieu, D.; Sanche, L. Concomitant treatment of F98 glioma cells with new liposomal platinum compounds and ionizing radiation. *J. Neuro-Oncol.* **2010**, *97* (2), 187−193.
(48) Olive, P. L.; Banáth, J. P. Kinetics of H2AX phosphorylation after exposure to cisplatin. *Cytometry, Part B* **2009**, *76B* (2), 79−90.
(49) Pitek, A. S.; Jameson, S. A.; Veliz, F. A.; Shukla, S.; Steinmetz, N. F. Serum albumin 'camouflage' of plant virus based nanoparticles prevents their antibody recognition and enhances pharmacokinetics. *Biomaterials* **2016**, *89*, 89−97.
(50) Gulati, N. M.; Pitek, A. S.; Steinmetz, N. F.; Stewart, P. L. Cryo-electron tomography investigation of serum albumin-camouflaged tobacco mosaic virus nanoparticles. *Nanoscale* **2017**, *9* (10), 3408−3415.
(51) Bludau, H.; Czapar, A. E.; Pitek, A. S.; Shukla, S.; Jordan, R.; Steinmetz, N. F. POxylation as an alternative stealth coating for biomedical applications. *Eur. Polym. J.* **2017**, *88*, 679−688.
(52) Creager, A. N.; Scholthof, K. B.; Citovsky, V.; Scholthof, H. B. Tobacco mosaic virus. Pioneering research for a century. *Plant Cell* **1999**, *11* (3), 301−8.
(53) Pitek, A. S.; Wen, A. M.; Shukla, S.; Steinmetz, N. F. The Protein Corona of Plant Virus Nanoparticles Influences their Dispersion Properties, Cellular Interactions, and In Vivo Fates. *Small* **2016**, *12* (13), 1758−1769.
(54) Singh, P.; Kim, Y.-J.; Zhang, D.; Yang, D.-C. Biological Synthesis of Nanoparticles from Plants and Microorganisms. *Trends Biotechnol.* **2016**, *34* (7), 588−599.
(55) Mehta, S.; Jayeeta; Shastri, V.; H, M. Recent Advancement in PLGA Nano Polymer Synthesis and its Applications. *J. Nanomed Res.* **2016**, *4* (1), 76.


DOI: 10.1021/acs.molpharmaceut.7b00466
*Mol. Pharmaceutics* XXXX, XXX, XXX−XXX